REPORT DOCUMENTATION PAGE

Form Approved
OMB No. 0704-0188

1. REPORT DATE *(DD-MM-YYYY)*
30-Sep-2008

2. REPORT TYPE
REPRINT

3. DATES COVERED *(From - To)*

4. TITLE AND SUBTITLE
ANALYSIS AND SIMULATION OF 3D SCATTERING DUE TO HETEROGENEOUS CRUSTAL STRUCTURE AND SURFACE TOPOGRAPHY ON REGIONAL PHASES, MAGNITUDE AND DISCRIMINATION

5a. CONTRACT NUMBER
FA8718-07-C-0003

5b. GRANT NUMBER

5c. PROGRAM ELEMENT NUMBER
62601F

6. AUTHOR(S)
Arben Pitarka[1], Don V. Helmberger[2], and Sidao Ni[1]

5d. PROJECT NUMBER
1010

5e. TASK NUMBER
SM

5f. WORK UNIT NUMBER
A1

7. PERFORMING ORGANIZATION NAME(S) AND ADDRESS(ES)
URS Group, Inc.
200 Orchard Ridge Drive, Suite 101
Gaithersburg, MD 20878-1978

8. PERFORMING ORGANIZATION REPORT NUMBER

9. SPONSORING / MONITORING AGENCY NAME(S) AND ADDRESS(ES)
Air Force Research Laboratory
29 Randolph Road
Hanscom AFB, MA 01731-3010

10. SPONSOR/MONITOR'S ACRONYM(S)
AFRL/RVBYE

11. SPONSOR/MONITOR'S REPORT NUMBER(S)
AFRL-RV-HA-TR-2008-1082

12. DISTRIBUTION / AVAILABILITY STATEMENT
Approved for Public Release; Distribution Unlimited.

URS Group[1] and California Institute of Technology[2]

13. SUPPLEMENTARY NOTES
Reprinted from: Proceedings of the 30th Monitoring Research Review – Ground-Based Nuclear Explosion Monitoring Technologies, 23 – 25 September 2008, Portsmouth, VA, Volume I pp 201 - 212.

14. ABSTRACT
The main purpose of this study is the understanding of scattering and its effects through step-by-step numerical experiments and waveform modeling, with the goal of providing useful insights into ongoing research for the development of simple empirical models of scattering that can be used in reducing the scatter in measures of Lg and coda wave magnitude and for discrimination purposes as well. We are performing anelastic 3D finite-difference simulations of wave propagation in highly heterogeneous media for a range of source depths, receiver distances and source types. In the first stage of our study we investigated the effect of small-scale crustal heterogeneities on wave propagation scattering. During the second stage we investigated the effect of surface topography combined with crustal heterogeneities on wave propagation scattering. In our simulations of regional wave propagation we used a finite difference computer program using our computer cluster. The seismograms were calculated at up to 3.5 Hz for regional distances of up to 300 km. The topography elevation was simulated using correlated random variations along the free surface. Our simulations show that the surface topography increases the wave-path scattering effects. The combined effects of crustal heterogeneities and surface topography produce Lg, P, and S coda waves with significant energy even for explosion sources. The energy of Lg coda waves depends on the source depth. P/Lg ratios estimated at different frequencies indicate that this ratio could be a good discriminant between explosions and earthquakes when calculated at high frequencies. The wave-path scattering effects were also investigated by simulating observed high frequency source directivity effects, as well as fault zone wave trapping in highly fractured conditions from aftershocks of the Big Bear earthquake sequence.

15. SUBJECT TERMS
Synthetic seismograms, Seismic scattering, Seismic magnitude, Seismic discrimination

16. SECURITY CLASSIFICATION OF:			17. LIMITATION OF ABSTRACT	18. NUMBER OF PAGES	19a. NAME OF RESPONSIBLE PERSON
a. REPORT	b. ABSTRACT	c. THIS PAGE			Robert J. Raistrick
UNCLAS	UNCLAS	UNCLAS	SAR	12	19b. TELEPHONE NUMBER *(include area code)* 781-377-3726

ANALYSES AND SIMULATION OF 3D SCATTERING DUE TO HETEROGENEOUS CRUSTAL STRUCTURE AND SURFACE TOPOGRAPHY ON REGIONAL PHASES, MAGNITUDE DISCRIMINATION

Arben Pitarka[1], Don V. Helmberger[2], and Sidao Ni[1]

URS Group[1] and California Institute of Technology[2]

Sponsored by Air Force Technical Applications Center

Contract No. FA8718-07-C-0003
Proposal No. BAA08-39

ABSTRACT

The main purpose of this study is the understanding of scattering and its effects through step-by-step numerical experiments and waveform modeling, with the goal of providing useful insights into ongoing research for the development of simple empirical models of scattering that can be used in reducing the scatter in measures of Lg and coda wave magnitude and for discrimination purposes as well. We are performing anelastic 3D finite-difference simulations of wave propagation in highly heterogeneous media for a range of source depths, receiver distances and source types. In the first stage of our study we investigated the effect of small-scale crustal heterogeneities on wave propagation scattering. During the second stage we investigated the effect of surface topography combined with crustal heterogeneities on wave propagation scattering. In our simulations of regional wave propagation we used a finite difference computer program using our computer cluster. The seismograms were calculated at up to 3.5 Hz for regional distances of up to 300 km. The topography elevation was simulated using correlated random variations along the free surface. Our simulations show that the surface topography increases the wave-path scattering effects. The combined effects of crustal heterogeneities and surface topography produce Lg, P, and S coda waves with significant energy even for explosion sources. The energy of Lg coda waves depends on the source depth. P/Lg ratios estimated at different frequencies indicate that this ratio could be a good discriminant between explosions and earthquakes when calculated at high frequencies. The wave-path scattering effects were also investigated by simulating observed high frequency source directivity effects, as well as fault zone wave trapping in highly fractured conditions from aftershocks of the Big Bear earthquake sequence.

OBJECTIVES

Our objective is to analyze and evaluate the effect of scattering on the amplitude and frequency content of Pg, Rg, and Lg waves due to small-scale crustal heterogeneities and surface topography by three-dimensional (3D) finite-difference simulations and modeling of recorded waveform data. During this phase of our research we focused on the following topics:

1. Influence of scattering due to complex structure and surface topography on the variability observed in amplitude estimates of regional phases. We analyzed simulation results of regional wave propagation scattering, obtained with an efficient 3D finite-difference computer program executed on a computer cluster at the California Institute of Technology, using message passing interface (MPI) .
2. Influence of source emplacement conditions on scattering of P and S waves for explosion sources located inside and outside shallow basins.

RESEARCH ACCOMPLISHED

Crustal heterogeneities of all scales and surface topography are shown to be very important factors influencing the scattered waves observed as coda arriving after the main wave phases. Some of their robust features such as amplitude and duration are related to the source itself, and location. Therefore different types of coda waves are being used for moment estimates for small event and source discrimination as well. The origin and the characteristics of the wave propagation scattering need to be investigated by both observational and numerical techniques. While analyses of recorded seismograms can reveal the degree of complexities in the crust and the effect of small- and large-scale perturbation on different wave phases, the numerical experiments can be used for isolating effects caused by the wave path, seismic source, and local structures. They can also be used to verify hypotheses that are at the foundation of several discrimination methodologies and complement studies of waveform analyses in regions with sparse station coverage.

The regional discriminants and magnitude methods rely mainly on the general feature of decreased S-phase amplitude and increase of P-phase amplitudes for explosion sources. However explosions produce anomalous large s-phase amplitudes that confound regional methods. It is therefore important to understand the factors that are at the origin of such behavior. In this study we investigate one factor: the effect of scattering due to random heterogeneities in the upper crust on the local and regional wavefield from explosion and earthquake sources.

In this study we apply a 3D staggered grid finite difference technique and a grid with variable spacing to simulate the effect of surface topography and shallow crustal heterogeneity on wave propagation scattering on both isotropic explosion and earthquake sources. Random fluctuations of wave speed and topography modeled with exponential averaging controlled by correlation lengths are used in generating crustal velocity models. In addition to simulated waveforms we analyzed smoothed envelopes of recorded waveforms from selected earthquakes and explosions in North Korea, recorded at regional stations with different wave-path scattering conditions. Our analyses show that the coupling between the surface and body waves, phase changes due to shallow wave propagation scattering, and local conditions in the source region significantly influence the amplitude of P and S coda waves as well as Rg waves. Such influence is frequency- and source-type dependent. Therefore, numerical experimention can help design efficient discriminantion procedures between earthquakes and explosions by using distant stations where the scattering removes the effects of Rg.

Parameterization of Scattering Models

We have developed a regional seismic wave numerical modeling method to investigate wave scattering due to shallow crustal heterogeneity and free surface topography for explosion and earthquake sources. Our initial work has been focused on small-scale shallow crustal heterogeneity effects by using models with flat free surface. Now we have extended our study to more complex crustal structures that include complex surface topography.

The spatial perturbation of velocity in our 3D model is expressed as a percentage of the unperturbed shear modulus μ. The random perturbations are intercorrelated using a spatial correlation length D. The perturbed shear modulus μ^* at each given grid node 'k' is calculated using the following equation:

$$\mu_k^* = \mu_k(1+0.35f_k)$$

where,

$$f_k = \frac{\sum_1^N \omega_i * rand_i}{W_k} \qquad W_k = \sum_1^N \omega_i \qquad \omega_i = \exp(-\frac{d_i}{D})$$

– $rand_i$: a spatial distribution of real random numbers ranging between -1 and 1.
– d_i: distance between the given node 'k' and adjacent nodes located within an ellipsoid centered at node 'k' with horizontal long axis D and short axis D/2.
– D: correlation length. D = 1.5 km.

The scattering parameters, such as the amount of perturbation and its correlation, were derived during the previous phase of this study. Velocity perturbation of up to 8% with a correlation length of 1.5 km was found to correctly reproduce the observed P and S coda waves' decay and the disappearance of their corresponding frequency-dependent radiation pattern. An example of scattering effect on observed P- and S-wave propagation, expressed as amplitude variation of the ground velocity envelope, is illustrated in Figure 1. This figure shows the amplitude variation of the ground velocity envelope as a function of frequency from the Mw4.5 070120 earthquake in South Korea. We used broad-band recordings at station CHC, CHJ, ULJ, and SES. The pure strike-slip mechanism of the earthquake and its recording at stations near the P wave nodal planes are ideal for analyzing regional scattered waves. Stations CHJ and CHC are close to P-wave nodal planes. The P wave scattering, expressed as the relative increase of amplitude of the P wave and its coda in the tangential component of motion at P-wave nodal stations, becomes significant at frequencies higher than 4 Hz. Note the relatively large amplitude of P coda waves on the tangential component at such frequencies. This indicates that high-frequency P- to S-wave conversions are significant. It is important to note that scattering effects due to small-scale perturbation in the shallow crust cause the increase in amplitude of high frequency P-wave coda in all three components. Because of their shorter wavelength, S waves are more susceptible to wave propagation scattering effects. As shown in Figure 1, for such waves, the amplitude difference between the three components that is controlled by the source radiation pattern is observed only at frequencies lower than 2 Hz. In general, at higher frequencies the amplitude of S wave coda is mainly controlled by scattering. Consequently it is the same for all three components. These observed features of P and S phases can help constrain scattering parameterization.

Analyses of Scattering Effects on Observed Waveforms

The origin of the high frequency scattering affecting mainly the P, Rg, and Lg coda waves (above 1 Hz) could be due to either deep or shallow crustal structure complexities along the wave path or in the source region (e.g., Dainty 1996; Wu et al., 2000, He et al., 2008). Lg waves show evidence of scattering from small-scale structures. Other causes of scattering could also be large-scale structural complexities such as crustal thinning or multipathing in the crust and large basins (e.g., Ni and Barazangi, 1983; Phillips et al., 2000).

Figure 3a shows smoothed envelopes of broad-band velocity seismograms from the 020416 earthquake in North Korea, recorded at station MDJ (Figure 2) and at a station located southwest of MDJ named STATION1. The epicentral distances of STATION 1 and MDJ are about 100 km and 400 km, respectively. The envelopes are calculated at the frequency bands of 0.8-2 Hz and 4-8 Hz. An interesting feature of the envelopes is the decay rate of P coda waves. At STATION 1 the decay rate is much higher than that at MDJ. Also in contrast with MDJ, at STATION1 the amplitude ratio between P and S waves does not change with frequency. These two observations suggest that in the considered region the wave propagation scattering is azimuthally dependent. Scattering is stronger along the path to MDJ, which is also the longest. As a consequence the S/P ratio at MDJ is strongly reduced at high frequencies in all three components.

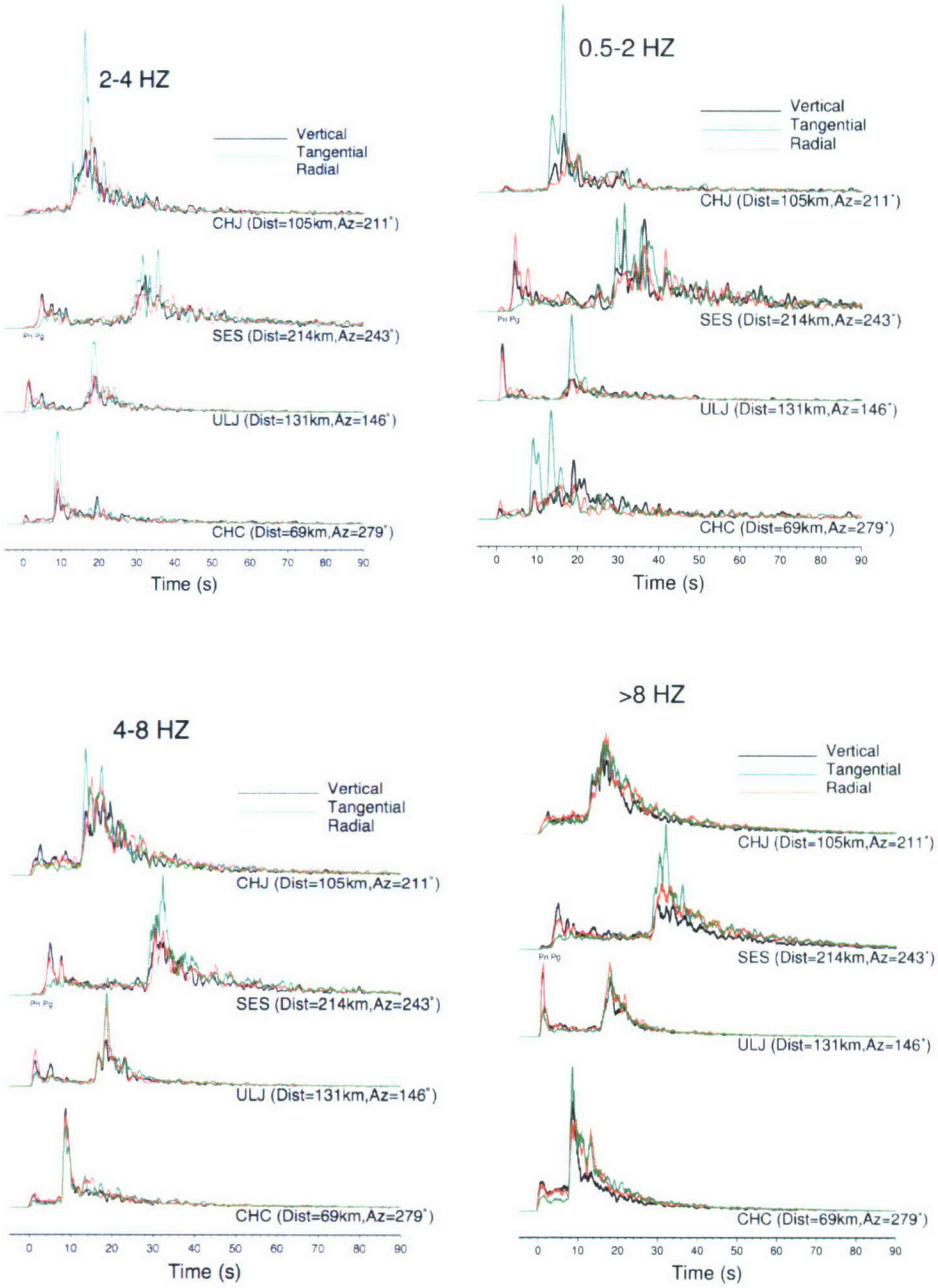

Figure 1. Smoothed envelopes of broad-band velocity seismograms recorded at station CHJ, SES, ULJ, and CHC from the Mw4.5 070120 earthquake in South Korea. The envelopes are calculated at four frequency bands indicated on top of each panel. Color traces show different components. The epicentral distance and azimuth are indicated at each trace. Note the large amplitude of the P wave on the vertical and radial components at stations CHJ, SES, and ULJ, which are located near the nodal planes. The difference in the P wave seen among the three components is caused by the source radiation. It is preserved only at frequencies up to 4 Hz. In general, at frequencies higher than 4 Hz, the amplitude of P-wave coda become the same at all components. This is a clear indication of scattering effects in the shallow crust.

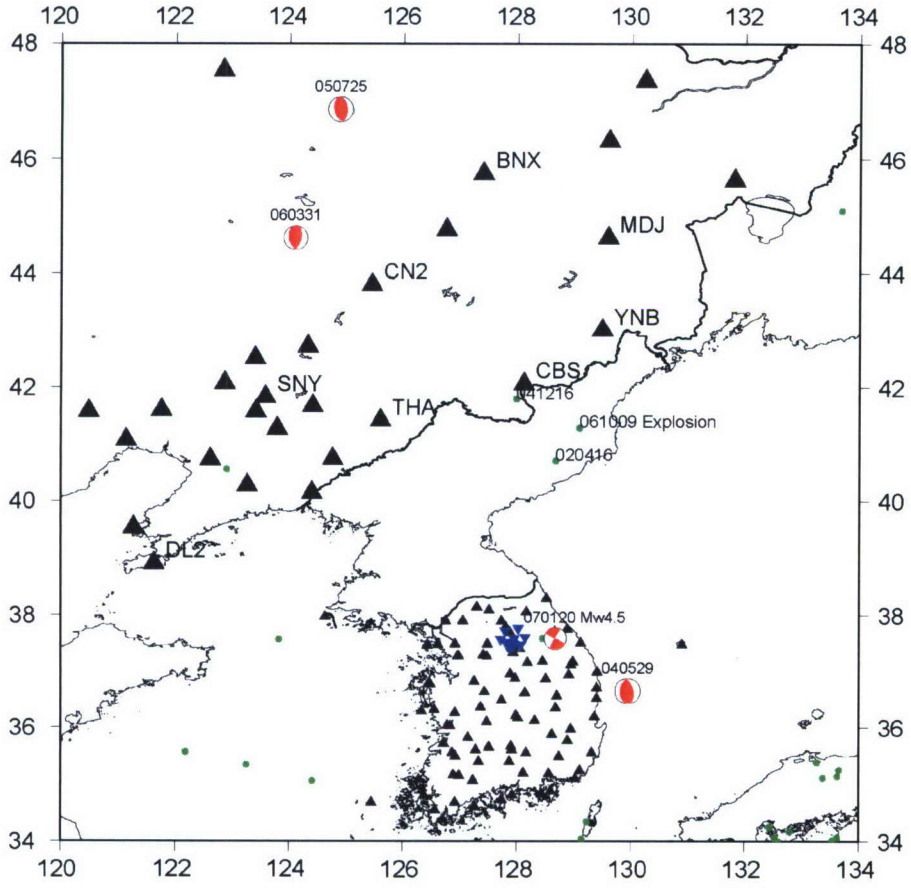

Figure 2. Map indicating stations and events (M>4) in China, the Korea Peninsula and adjacent regions considered in this study. Triangles indicate broadband and short period stations of the China Seismic Network and Korean Seismic Network, and the blue inverted triangles indicate IMS stations (KSRS). The 061009 explosion and 020416 earthquake located in the Korean peninsula and analyzed in this study are shown by green dots.

Figure 3b shows smoothed waveform envelopes for the 061009 North Korean explosion calculated at MDJ and STATION1. The explosion waveforms are rich in S wave energy, in particular at STATION1, which is closer to the source. The difference in wave scattering between the two stations remains visible even for the explosion source. which is much shallower than the earthquake. This suggests that the difference in scattering effects between the two stations is rather shallow and not strictly related to the source region.

The comparison of waveform envelopes between the earthquake and explosion is shown in Figure 4. At STATION1 with low wave path scattering the P/S coda waves amplitude ratio is the same for both earthquake and explosion. In contrast at MDJ the P/S ratio between the earthquake and explosion is very different. The P/S ratio for the explosion is much stronger. These observations suggest that at large epicentral distances for which the cumulative effect of wave scattering is enhanced, the P/S coda wave ratio could be a good discriminant between earthquakes and explosions.

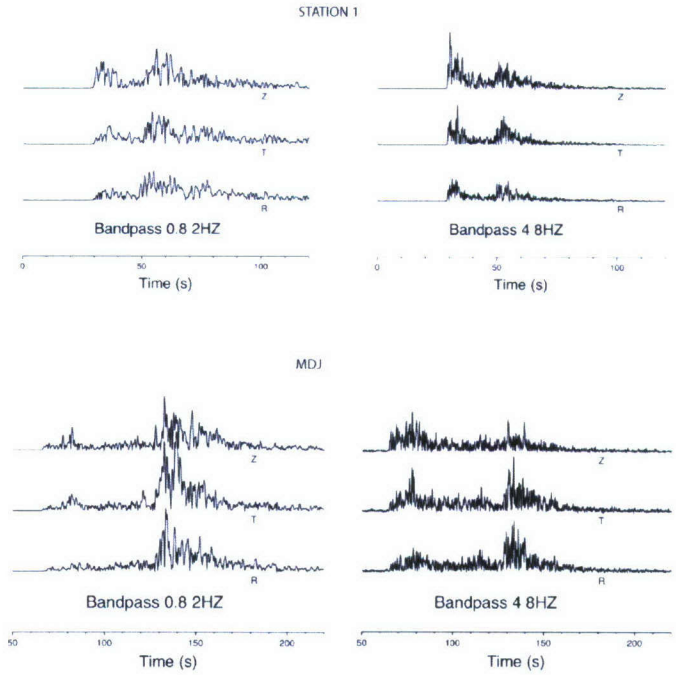

Figure 3a. Smoothed envelopes of velocity seismograms from the 020416 earthquake in North Korea recorded at STATION 1 (top panels) and MDJ (bottom panels) in the frequency ranges 0.8–2 Hz and 4–8 Hz.

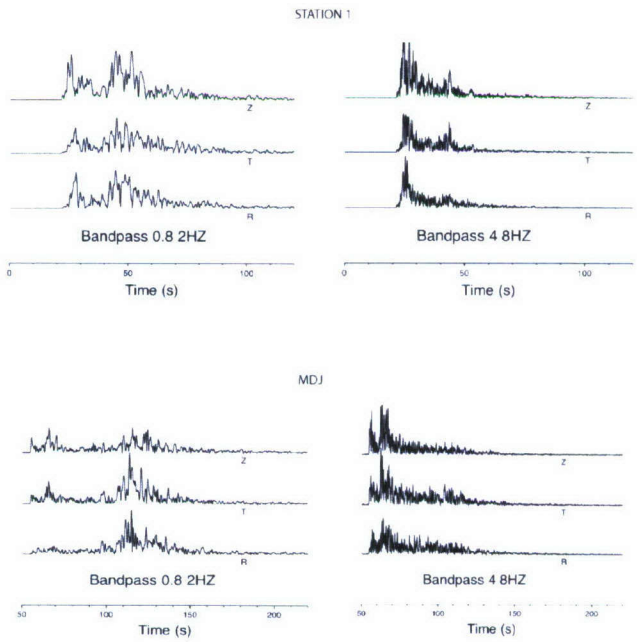

Figure 3b. Smoothed envelopes of velocity seismograms from the 061009 North Korean explosion recorded at STATION 1 (top panels) and MDJ (bottom panels) in the frequency ranges 0.8–2 Hz and 4–8 Hz.

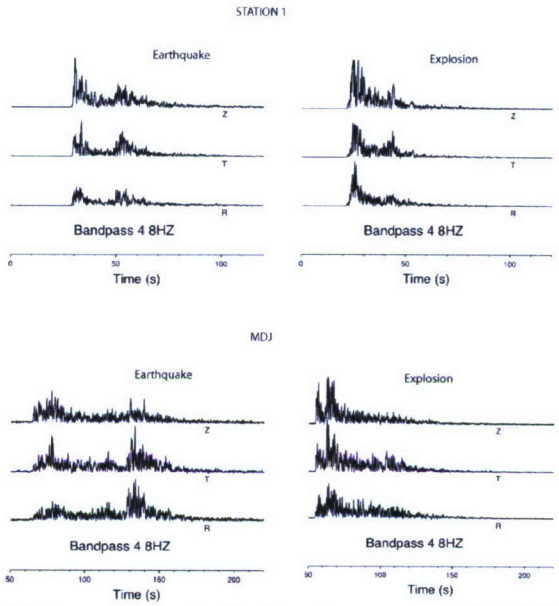

Figure 4. Comparison of smoothed envelopes of velocity seismograms at STATION1 and MDJ from the 020416 earthquake (left panels) and 061009 explosion (right panels) in North Korea, band-pass filtered at 4–8 Hz. Note that along the short wave path to STATION1 P/S amplitude ratios for the earthquake and explosion are very similar. In contrast along the wave path to MDJ, which is longer, and with strong wave scattering, the P/S ratios between the earthquake and explosion are very different. At MDJ the P/S ratio for the explosion is much larger. This suggests that at large epicentral distances and in a strong scattering environment, the two types of sources discriminate very well.

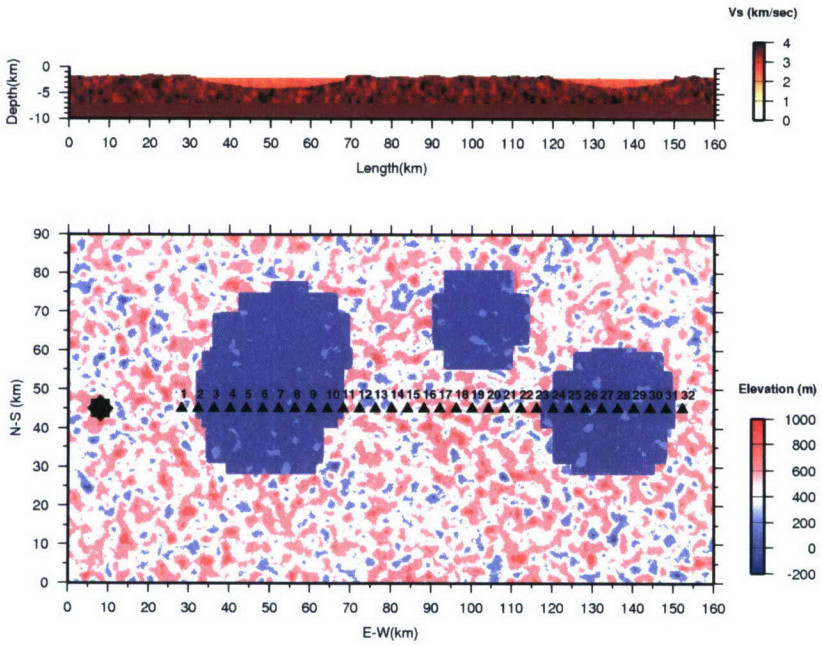

Figure 5. Velocity model with smooth topography used in simulations of wave propagation scattering.
Top Panel: Cross section of the top 7 km of the velocity model along the source-station linear array. The velocity is randomly perturbed in the upper 5 km of the crust.
Bottom Panel: Topography elevation and stations (triangles) and epicenter (star) locations.

Simulated Scattering

Numerical modeling can establish a link between the observed frequency-dependent effects of scattering and their physical explanation. During this second phase of our study we have examined combined effects of wave propagation scattering due to complexities in the shallow crust and surface topography. We have calculated synthetic seismograms for earthquake and explosion point sources using a parallelized 3D finite-difference code (Pitarka,1999). Our finite difference code solves the stress-velocity wave equations in a heterogeneous medium using staggered grids. The technique for generating the 3D velocity model on a regular grid with variable spacing allows for inclusion of small-scale complexities and surface topography as well. The technique we use to model free surface topography is an extension of the formalism that we have applied to modeling wave propagation in media with a curved free surface (Pitarka and Irikura,1996). The performance of our free-surface boundary condition technique at handling Lg coda waves for a flat free surface and very long distances was compared with that of the FK method of Saikia (1994) for a shallow source. Also, the technique has been validated against other standard and accurate techniques for modeling surface topography such as the 2D-Boundary Element Method (BEM) and the 2D-Discrete Wavenumber-Boundary Integral Equation method of Takenaka et al. (1996).

We looked at the relative contribution of wave-field scattering on different frequency bands of P, Rg and Lg coda waves due to surface topography and localized and highly heterogeneous small scale bodies embedded in a reference planar layered velocity model that was used in modeling regional wave propagation in the South Korea region (Kim, 1995). The small-scale variations of the velocity are randomly distributed along the top 5km of the crust. In addition to the small-scale fluctuations our velocity model includes several microbasins with sizes varying between 10-25 km and depth up to 4 km. The velocity fluctuations are in the range of 2-8% and their correlation length is 1.5 km. The elevation of surface topography varies between 0 and 800m. The correlation length of topography random variations is 3.5 km. The selected minimum grid spacing of 200 m ensures accurate wave propagation modeling up to 3.0 Hz. The 3D model occupies a volume of 160x90x20 km. The ground motion velocity was computed on a linear array of stations located on the free surface. The stations spacing is 20 km, and the maximum epicentral distance is 146 km. Several stations are located in basins.

Aiming at understanding scattering effects in relation to the source type we performed simulations for an explosion point source located at a depth of 400 m, and earthquake double-couple point sources located at a depth of 7 km. Since we are looking at indirect mechanisms of S wave generation, mainly wave-path scattering, we used the isotropic representation of the explosion source in our simulations. The source time function for both earthquake and explosion has a flat spectrum in the considered frequency range.

A cross section of the velocity model and free-surface topography used in the simulations is shown in Figure 5. Figure 6 shows the difference in waveform characteristics between the earthquake and explosion. We compared the vertical component of synthetic velocity seismograms calculated at a linear array of receivers for a strike slip earthquake located at a depth of 7 km. The strike angle of the fault is 90^{o} and the rake angle is 50^{o}. It is obvious that shallow random complexities create coda waves with long duration. The S and Lg coda waves are very energetic even at short distances. The effects of the shallow heterogeneities on wave type conversions such as P to S and S to P as well as on Rg waves are impressive, especially for the explosion source that does not emit S waves. Our numerical experiment clearly shows that wave-path scattering alone caused by rough topography and crustal heterogeneities can produce Lg, P, and S coda waves with significant energy even for explosion sources. The Rg wave dominates the later phases in explosion seismograms. Their amplitude is larger than that of the direct P wave. However, at high frequencies (above 1 Hz) the Rg waves quickly attenuate with distance. Because of the Rg to Lg conversions caused by the surface topography, the amplitude of Rg waves is comparable with that of the P waves (see Figure 6b). As demonstrated by the comparison of smoothed envelopes of waveforms calculated at selected stations (Figure 7), P coda waves from the explosion remain strong. The cumulative effect of scattering caused by the surface topography and spatial structural heterogeneities contributes to the generation of P coda waves through P/S and S/P conversions. At high frequencies, the difference in the P/Rg ratio between the explosion and the earthquake source is significant. The P/Rg wave ratio could be a good discriminant when the earthquake is not very shallow and the explosion is not located near a complex boundary (e.g., Saikia, 1992).

(a) 0.1–2.5 Hz **(b) 1.0–2.5 Hz**

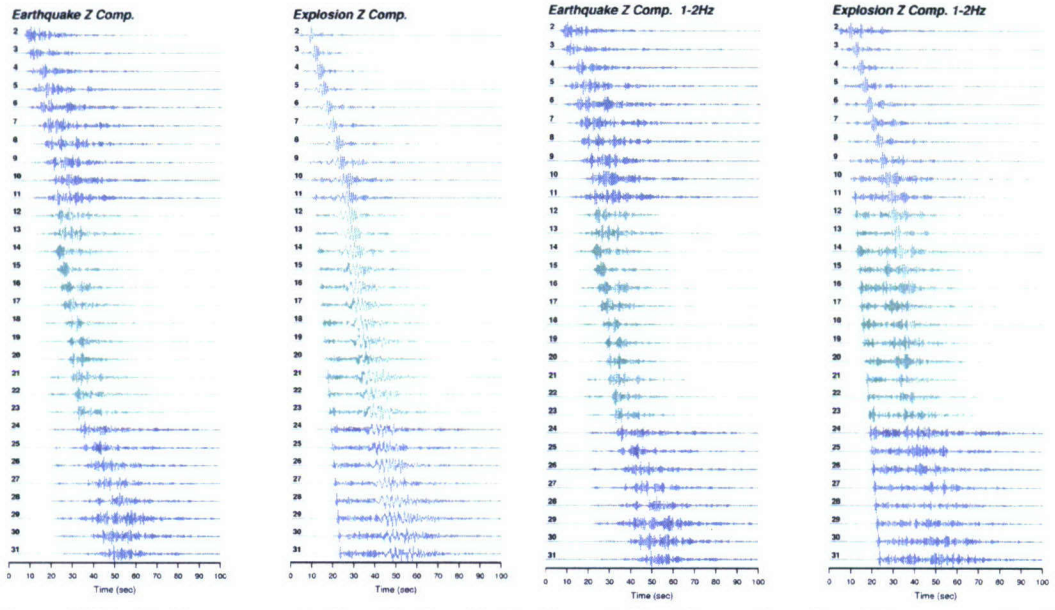

Figure 6. Vertical component of synthetic velocity for a strike-slip earthquake with a source depth of 7 km (left panel) and an isotropic explosion source at a depth of 0.4 km (right panel). The synthetic seismograms are calculated with a 3D model that includes shallow crustal scattering effects. (a) Band-pass filtered at 0.1–2.5 Hz (b) Band-pass filtered at 1.0–2.5 Hz. All synthetics are scaled to their individual maximum amplitude in order to enhance the relative amplitude of P and S waves at each station. Note the impressive energy of S and Rg coda waves developed for an explosion source.

(a) 0.1–0.5 Hz **(b) 1.0–2.5 Hz**

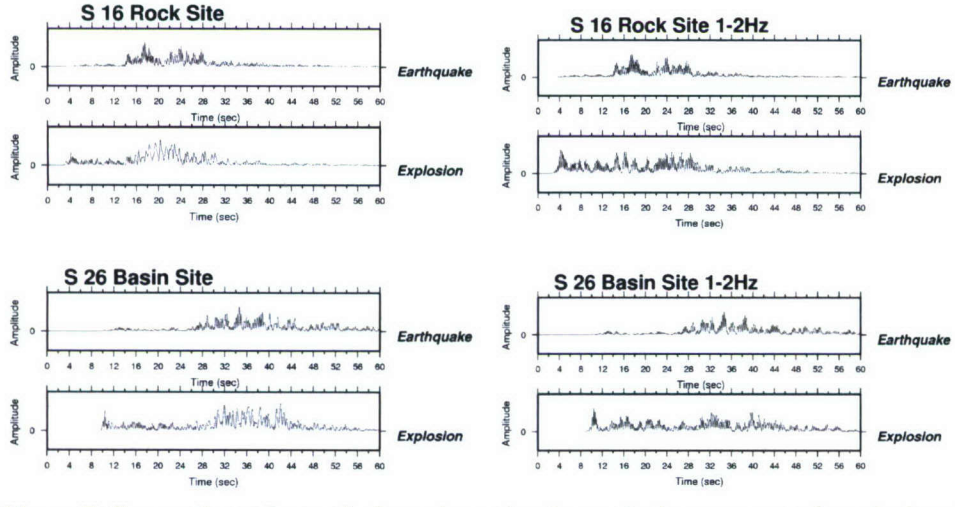

Figure 7. Comparison of smoothed envelopes for the vertical component of synthetic velocity seismograms at a rock site (station 16) and basin site (station 26) for the earthquake and explosion sources. Note the relatively large P/S ratio of coda waves for the explosion. P/S ratio increases with the frequency, making it a good discriminant.

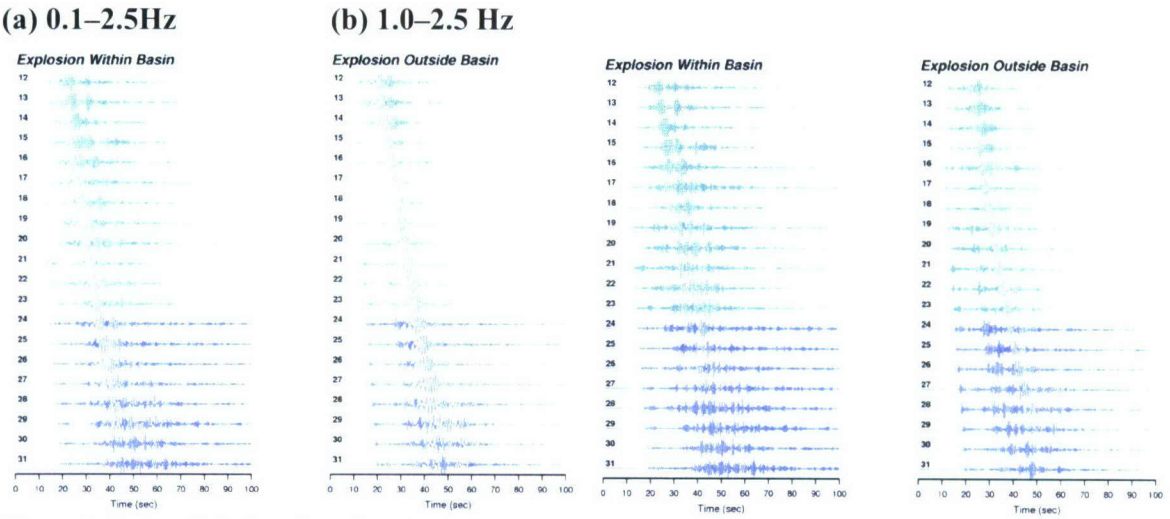

Figure 8. Effect of the location of explosion source with respect to basin edge on wave scattering. Comparison of vertical component velocity seismograms for an explosion source located near the basin edge inside the basin (left panel) and outside the basin (right panel). (a) Band-pass filtered at 0.1–2.5 Hz (b) Band-pass filtered at 1.0–2.5 Hz. Note that because of the wave trapping within the basin, the S-wave coda for the explosion inside the basin are more pronounced. In contrast, the amplitude of P and P coda waves is reduced, especially at high frequencies.

Emplacement Effects

Figure 8 compares the simulated vertical component of velocity for explosion sources located near the basin edge, inside and outside a basin. The explosion outside the basin produces much larger P waves that are rich in high frequencies. In contrast the amplitude of the P wave and P coda waves is relatively small for the basin explosion. In this case the energy reduction of the P wave is caused by P to S conversions. Besides being attenuated in the basin sediments, the P waves do not develop much coda wave, as some of their energy that is reflected at the free surface leaks back to the underlying bedrock and deeper crust and probably is subject to trapping and intrinsic attenuation. As a consequence, the waveforms from the basin explosion look very similar to those from an earthquake. This is clearly seen in both Figure 9 and Figure 10 where we compare smoothed envelopes of synthetic waveforms in the frequency range 1.0–2.5 Hz. Our simulation suggests that P/Rg ratio for explosion sources is sensitive to the source emplacement.

CONCLUSIONS AND RECOMMENDATIONS

Our numerical experiments with 3D velocity models that include surface topography, random velocity perturbations and microbasins, representing wave scattering in the upper 5 km of the crust, clearly show that wave-path scattering is a major contributor to S and Lg coda waves from explosions at regional distances. Explosion sources generate strong Rg waves. The energy of the Rg waves depends on distance and wave propagation scattering. Strong scattering and its cumulative effect at long distances breaks down Rg waves while still contributing to the creation of P coda waves. As a consequence, at regional distances and high frequencies, the P/Rg ratio is larger for explosions than for earthquakes. The amplitude of P waves and P coda waves from explosions depends on the source emplacement. Our simulations suggest that at large distances P waves generated from basin explosions located near the basin edge are relatively weak. Consequently, P/Rg ratios for such events could be very similar to earthquakes.

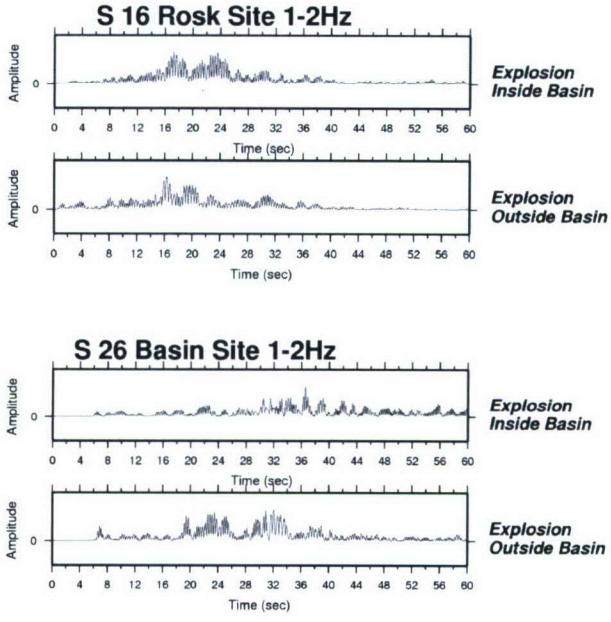

Figure 9. Comparison of smoothed envelopes for the vertical component of synthetic velocity seismograms at a rock site (station 16) and a basin site (station 26) for explosion sources inside and outside the basin. Note that at longer distances (station 26) the two different source inplacements produce S coda waves with very different characteristics. The amplitude of S coda waves for the source inside the basin is reduced significantly.

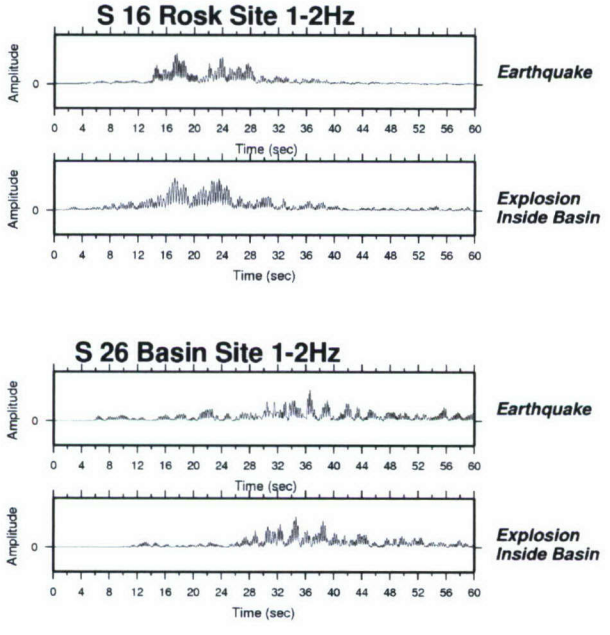

Figure 10. Comparison of smoothed envelopes for the vertical component of synthetic velocity seismograms at a rock site (station 16) and basin site (station 26) for an earthquake source and explosion source located inside the basin. Note that for such a location of the explosion source and the considered frequency range, using P/Rg ratio to discriminate between an earthquake and an explosion becomes difficult.

REFERENCES

Dainty, A. (1996). The influence of seismic scattering on monitoring, in *Monitoring a Comprehensive Test Ban Treaty*. NATO Science Series. Springer: pp. 663–688.

Goff, J. A. and T. H. Jordan (1988). Stochastic modeling of seafloor morphology: Inversion of sea beam data for second-order statistics, *J. Geophys. Res.* 93: 13589–13608.

He, Y., X. Xie, and T. Lay (2008). Explosion-source energy partitioning and Lg-wave excitation: Contributions of free-surface scattering, *Bull. Seism. Soc. Am.* 98: 778–792.

Kim, W. and P. G. Richards. North Korean nuclear test: Seismic discrimination at low yield, *Trans. Am. Geophys. U.* 88: 158–161.

Mayeda, K. M., A. Hofstetter, J. L. O'Boyle, and W. R. Walter (2003). Stable and transportable regional magnitudes based on coda-derived moment rate spectra, *Bull. Seis. Soc. Am.* 93: 224–239.

Myers, C. S., J. Wagoner, L. Preston, K. Smith, H. Tkalcic, and S. Larsen (1996). The effect of realistic geologic heterogeneity on local and regional P/S amplitude ratios based on numerical simulations, in *Proceedings of the 28th Seismic Research Review: Ground-Based Nuclear Explosion Monitoring Technologies*, LA-UR-06-5471, Vol. 1, pp. 146–155.

Ni, J. and M. Barazangi (1983). High frequency seismic wave propagation beneath the Indian shield, Himalayan Arc, Tibetian Plateau, and surrounding regions: High uppermost mantle velocities and efficient Sn propagation beneath Tibet, *Geophys. J. Int.* 72: 655–689.

Phillips, W. S. and K. Aki (1986). Site amplification of coda waves from local earthquakes in central California, *Bull. Seism. Soc. Am.* 76: 627–648.

Phillips, W. S., H. E. Hartse, S. R. Taylor, and G. E. Randall (2000). 1 Hz Lg Q tomography in central Asia, *Geophys. Res. Lett.* 27: 3425–3428.

Pitarka, A. (1999). 3D elastic finite-difference modeling of seismic motion using staggered grid with nonuniform spacing, *Bull. Seis. Soc. Am.* 89: 54–68.

Pitarka, A. and K. Irikura (1996). Modeling 3D surface topography by finite-difference method: Kobe-JMA station site, Japan case study. *Geophys. Res. Lett.* 20: 2729-2732.

Saikia, C. K. (1994). Modified frequency-wave-number algorithm for regional seismograms using Filon's quadrature-modeling of L(g) waves in eastern North America, *Geophys. J. Int.* 118: 142–158.

Saikia C. (1992). Numerical study of quarry generated Rg as a discriminant for earthquakes and explosions: Modeling of Rg in southwestern New England. *J. Geophys. Res.* 97: 11057–11072.

Takenaka, H., B. L. Kennett, and H. Fujiwara (1996). Effect of 2-D topography and 3-D seismic wave field using a 2.5-D discrete wavenumber-boundary integral equation method, *Geophys. J. Int.* 124: 741–755.

Wu, Ru-Shan, S. Jin, and Xiao-Bi Xie (2000). Seismic wave propagation and scattering in heterogeneous crustal waveguides using screen propagators: I SH-waves, *Bull. Seismol. Soc. Am.* 90: 401–413.

Tan, Y., L. Zhu, D. V. Helmberger, and C. K. Saikia (2006). Locating and modeling regional earthquakes with two stations, *J. Geophys. Res.* 111: B01306, doi:10.1029/2005JB003775.

Xie, X., Z. Ge, and T. Lay (2005). Investigating explosion source energy partitioning and Lg-wave excitation using finite-difference plus slowness analyses method, *Bull. Seis. Soc. Am.* 95: 2412–2427.

Xie, X., T. Lay, and R. Wu (2005). Near-source energy partitioning for regional waves in 2D and 3D models, contributions of S^*-to-Lg and P-to-Lg scattering, in *Proceedings of the 27th Seismic Research Review: Ground-Based Nuclear Explosion Monitoring Technologies*, LA-UR-05-6407, Vol. 1, pp. 249–258.